

Entropic factors and structural motifs of triblock-terpolymer-based patchy nanoparticles

Nicolas Moreno, nicolas.morenoch@gmail.com
Burhannudin Sutisna
Eliot Fried, eliot.fried@oist.jp

Mathematics, Mechanics, and Materials Unit.
Okinawa Institute of Science and Technology, OIST

1 Experimental data

For the construction of the patchy nanoparticles we follow the methodology proposed by Müller and coauthors [1]. We use three different polymers for Poly(styrene-*b*-butadiene-*b*-methyl methacrylate) (SBM), Poly(styrene-*b*-isoprene-*b*-methyl methacrylate) (SIM), and Poly(styrene-*b*-isoprene-*b*-2-vinyl pyridine) (SIV). In Table SI 1 we give a breakdown of the molecular weights that we use to experimentally construct the patchy particles.

Table 1: Summary of triblock terpolymers used to construct the patchy particles. The subscripts indicates the molecular weight of each block

Code	Name	Polymer MW compositions
1	SBM1	PS _{30k} - <i>b</i> -PBd _{12k} - <i>b</i> -PMMA _{110k}
2	SBM2	PS _{22k} - <i>b</i> -PBd _{3.5k} - <i>b</i> -PMMA _{65k}
3	SBM3	PS _{20k} - <i>b</i> -PBd _{15k} - <i>b</i> -PMMA _{74k}
4	SIM1	PS _{58k} - <i>b</i> -PIP _{22k} - <i>b</i> -PMMA _{230k}
5	SIM2	PS _{105k} - <i>b</i> -PIP _{48k} - <i>b</i> -PMMA _{485k}
6	SIV1	PS _{29.5k} - <i>b</i> -PIP _{33.5k} - <i>b</i> -P2VP _{35k}
7	SIV2	PS _{36.5k} - <i>b</i> -PIP _{36.5k} - <i>b</i> -P2VP _{12k}

Parameter calculation and physical properties for experimental systems

To compute the Flory-Huggins pair interaction parameters for the different polymer-polymer and polymer-solvent components we use the Hansen [2] solubility parameters δ_I^d , δ_I^p , and δ_I^h for the I th species, with $I, J = A, B, C$, and S (see SI Table T1). The superscripts d , p , and h refer to the dispersive, polar, and hydrogen bonding contributions of the solubility parameters. The Flory-Huggins parameter χ_{IJ} can be computed as

$$\chi_{IJ} = \frac{v_{\text{ref}}}{RT} ((\delta_I^d - \delta_J^d)^2 + 0.25(\delta_I^p - \delta_J^p)^2 + 0.25(\delta_I^h - \delta_J^h)^2), \quad (1)$$

where $v_{\text{ref}} = 100\text{cm}^3/\text{mol}$ is a reference molar volume, $R = 3.14$ is the universal gas constant, and $T = 298.15\text{K}$ is the temperature. Computed values of the Flory-Huggins parameters are presented in SI Table 2.

We compute the number of repetitive units of each segment N_I for $I = A, B$, and C as $N_I = \mathcal{N}_I(v_I/v_{\text{ref}})$, where v_I is the molar volume of the different species and \mathcal{N}_I is the number of monomers per block.

Table 2: Molar volumes and Hansen solubility parameters for the different polymers and solvents used by Gröschel et al. [3] and Löbbling et al. [1]

Species	Molar volume	δ^d	δ^p	δ^h
Polystyrene	99.0	18.5	4.5	2.9
Polybutadiene	56.0	17.3	2.3	2.6
Polyisoprene				
Poly 2-vinyl pyridine				
Poly methyl metacrylate	139.4	18.6	10.5	5.1
Poly ter-butyl metacrylate	139.0	-	-	-
Acetone	74.0	15.5	10.4	7.0
Isopropanol	76.5	15.8	6.1	16.4

Table 3: Flory-Huggins interaction parameters

χ_{IJ}	PS	PB	PIP	P2VP	PMMA	PBM	Acet	IPA
PS	-	0.108			0.41	0.025	0.89	2.16
PB		-			0.81	0.007	0.99	2.16
PIP			-					
P2VP				-				
PMMA					-	-		
PBM						-	0.42	1.8
Acet							-	
IPA								-

Force and geometrical relations for spherical patches on spherical particles

We present the geometric analysis for a system consisting on a core, p patches and corona regions formed by the A, B , and C blocks. Strictly, the coronal region contains both solvent S and the swollen block C , however without loss of generality and to facilitate the presentation of the model, we consider the corona as an effective phase with properties of the corresponding C and solvent mixture. In the main document we label four distinctive regions with the index 1, 2, 3, and 4 to indicate the core, shell, corona, and surrounding solvent. Here to streamline our presentation we indicate each region with the index of their main constituent A, B , and C for the core, shell, and corona.

To start out the analysis we consider p spherical B patches located on the surface of a spherical A core with radii of curvature r_B and r_A , respectively. In Figure 1 we present a schematic of the nanoparticle. At the patch-core junction the radius of curvature is denoted by d . The surface tension between the core, patch, and surrounding corona are γ_{AB}, γ_{AC} , and γ_{BC} . The contact angles between the different regions are denoted by θ_A, θ_B , and θ_C , where $\theta_A + \theta_B + \theta_C = 2\pi$. For patchy nanoparticle at equilibrium, the junction between the spherical patch and core must satisfies force balance and geometrical constrains. As an additional assumption, we do not account for the connectivity between the blocks, thus, this description generalizes a situation where the force balance is driven by the surface tension between the species under the geometrical conditions presented.

Despite the assumptions on the force balance and geometrical constraints do not represent fully a patchy nanoparticle formed by triblock terpolymers, the characterization of a system on these conditions allow us to identify the natural dependence of the number of patches and interfacial areas in terms of the parameters conformational \bar{R}_1/\bar{R}_2 and interfacial parameters γ_{AB}/γ_{AC} presented in the main document.

Geometrical relations

For the spherical core and patch caps α_A and α_B are the curvature angles, respectively. Considering a flat patch-core interface the following relations holds for the curvature and contact angles $\theta_A = \pi - \alpha_A$, and $\theta_B = \pi - \alpha_B$. The assumption of flat interfaces is a good approximation for the triblock terpolymer systems here introduced. Generalizations to non-flat interfaces are acceptable under model that we present but require the definition of the apparent angle between the patch and the core as described by [?] for liquid droplets on solid surfaces with different curvature.

The following geometrical relations apply for the curvature radius d of the junction, $d = r_A \sin \alpha_A = r_B \sin \alpha_B$.

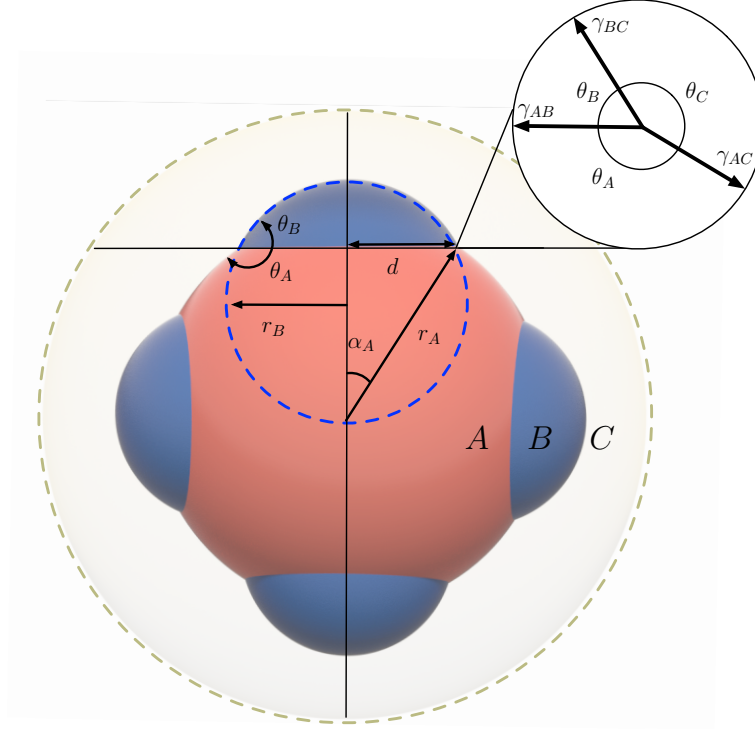


Figure 1: Cross section of a patchy nanoparticle with four patches. Our system consists on core, patches, and corona regions constituted by the A , B , and C blocks. The junction between the a spherical patch and core is presented.

Since $\theta_B = \pi - \alpha_A$, and $\theta_C = \pi - \alpha_B$, for a nanoparticle at the equilibrium we expect

$$r_B = r_A \frac{\sin(\theta_A)}{\sin(\theta_B)}. \quad (2)$$

The volume V_p of one patch is given by

$$V_p = \frac{4\pi}{3} r_B^3 \left(\frac{2 - 3 \cos \theta_B + \cos^3 \theta_B}{4} \right), \quad (3)$$

whereas the volume V_A of the core can be computed by subtracting the volume of the caps removed due to the presence of the p patches, from the volume of a sphere with radius r_A , leading to

$$V_A = \frac{4\pi}{3} r_A^3 \left(1 - p \frac{2 - 3 \cos(\pi - \theta_A) + \cos^3(\pi - \theta_A)}{4} \right). \quad (4)$$

The interfacial areas Ω_{AB} , Ω_{AC} , and Ω_{BC} between the core, shell, and corona can be defined as

$$\Omega_{AB} = p\pi d^2, \quad (5)$$

$$\Omega_{AC} = 2\pi r_A^2 (2 - p(1 - \cos(\pi - \theta_A))), \quad (6)$$

$$\Omega_{BC} = p2\pi r_B^2 (1 - \cos \theta_B), \quad (7)$$

where the second term in (6) correspond to the area of the caps removed from the core due to the presence of the patches.

Force balance

At equilibrium the contact line between the core, patch, and corona requires that the net force along it to be zero. If we consider that only surface tension effects are responsible for the equilibrium morphology, the force balance along each of the interfaces can be expressed as

$$\gamma_{BC} + \gamma_{AB} \cos \theta_B + \gamma_{AC} \cos \theta_C = 0, \quad (8)$$

$$\gamma_{BC} \cos \theta_B + \gamma_{AB} + \gamma_{AC} \cos \theta_A = 0, \quad (9)$$

$$\gamma_{BC} \cos \theta_C + \gamma_{AB} \cos \theta_A + \gamma_{AC} = 0. \quad (10)$$

In general, for stable junctions to exist between three domains i, j , and k the force balance imposes constraints in the magnitude of surface tension between the domains, such that $\gamma_{ij} < \gamma_{jk} + \gamma_{ik}$. If this condition is not satisfied the complete dewetting of one phase away from the other is expected. In the particular case of triblock copolymers the dewetting between chemically connected blocks cannot occur, and additional force contributions are expected as the polymer coil stretch to allocate in the different regions. Solving (8), (9), and (10) we can find the explicit dependence of $\cos \theta_A$ and $\cos \theta_B$ with the surface tensions

$$\cos \theta_A = \frac{1}{2} \frac{\gamma_{BC}^2 - \gamma_{AB}^2 - \gamma_{AC}^2}{\gamma_{AB}\gamma_{AC}}, \quad (11)$$

$$\cos \theta_B = \frac{1}{2} \frac{\gamma_{AC}^2 - \gamma_{AB}^2 - \gamma_{BC}^2}{\gamma_{AB}\gamma_{BC}} \quad (12)$$

Due to the force balance in the direction perpendicular to the junction (see Figure 1) we have

$$\gamma_{BC} \sin \theta_B = \gamma_{AC} \sin \theta_A, \quad (13)$$

thus from (2) we have that

$$\frac{r_B}{r_A} = \frac{\gamma_{BC}}{\gamma_{AC}} \quad (14)$$

Mass balance

Considering the patchy nanoparticles are formed by z triblock terpolymer chains with a total number of N repetitive units per chain, and N_A and N_B repetitive units per A and B block, respectively. Such that $N_C = N - N_A - N_B$ and that each repetitive unit has a reference volume v_{ref} , the total volume of the A and B blocks are $V_A = zv_{\text{ref}}N_A$ and $V_B = zv_{\text{ref}}N_B$. We can write the volumetric ratio between the blocks A and B as

$$V_B/V_A = pV_p/V_A = N_B/N_A. \quad (15)$$

Since N_B/N_A is constant for a given system, using the volumes V_p and V_A given by (3) and (4), and defining the function $f(\cos x) = (2 - 3 \cos(x) + \cos^3(x))/4$, the number of patches in a nanoparticle can be computed

$$p = \frac{V_B/V_A r_A^3}{r_B^3 f(\cos \theta_B) + V_B/V_A r_A^3 f(\cos(\pi - \theta_A))}. \quad (16)$$

Thus from (16) we can determine the number of patches from the parameters $\gamma_{AB}, \gamma_{AC}, \gamma_{BC}$, and V_B/V_A . This expression holds under the prescribed geometrical conditions of spherical patches on spherical core, thus the limit conditions in the number of patches for different surface tensions and volume fractions can indicate morphological transitions of the patches from spherical cap to rod-like.

To streamline the presentation and interpretation of our model we introduce the following dimensionless quantities

$$\tilde{\gamma}_{AB} = \frac{\gamma_{AB}}{\gamma_{AC}} \quad \tilde{\gamma}_{BC} = \frac{\gamma_{BC}}{\gamma_{AC}} \quad \tilde{r}_B = \frac{r_B}{r_A} \quad \tilde{d} = \frac{d}{r_A}. \quad (17)$$

Hence, using these dimensionless quantities and the relation (14), (11) and (12) can be written as

$$\cos \tilde{\theta}_A = \frac{1}{2} \left(\frac{1}{\tilde{\gamma}_{AB}} (\tilde{r}_B - 1) - \tilde{\gamma}_{AB} \right), \quad (18)$$

$$\cos \tilde{\theta}_B = \frac{1}{2} \left(\frac{1}{\tilde{r}_B \tilde{\gamma}_{AB}} - \frac{\tilde{\gamma}_{AB}}{\tilde{r}_B} - \frac{\tilde{r}_B}{\tilde{\gamma}_{AB}} \right). \quad (19)$$

replacing (18) and (19) in (16) we can identify that the number of patches can be written as a function of the dimensionless quantities $\tilde{\gamma}_{AB}$ and \tilde{r}_B

$$\tilde{p} = \frac{V_B/V_A}{\tilde{r}_B^3 f(\cos \tilde{\theta}_B) + V_B/V_A f(-\cos \tilde{\theta}_A)}. \quad (20)$$

We present in the main document the morphological transitions in the patches can be interpreted from the variation in the area Ω_{AB} between the core and patches. From (5) and using dimensionless quantities we can write

$$\Omega_{AB} = \tilde{p} \pi \tilde{d}^2 \quad (21)$$

The maximum number of patches that can be allocated in the nanoparticle while satisfying force and geometrical conditions can be approximated from the total surface area available in the core. In the limit condition $\Omega_{AC} = 0$

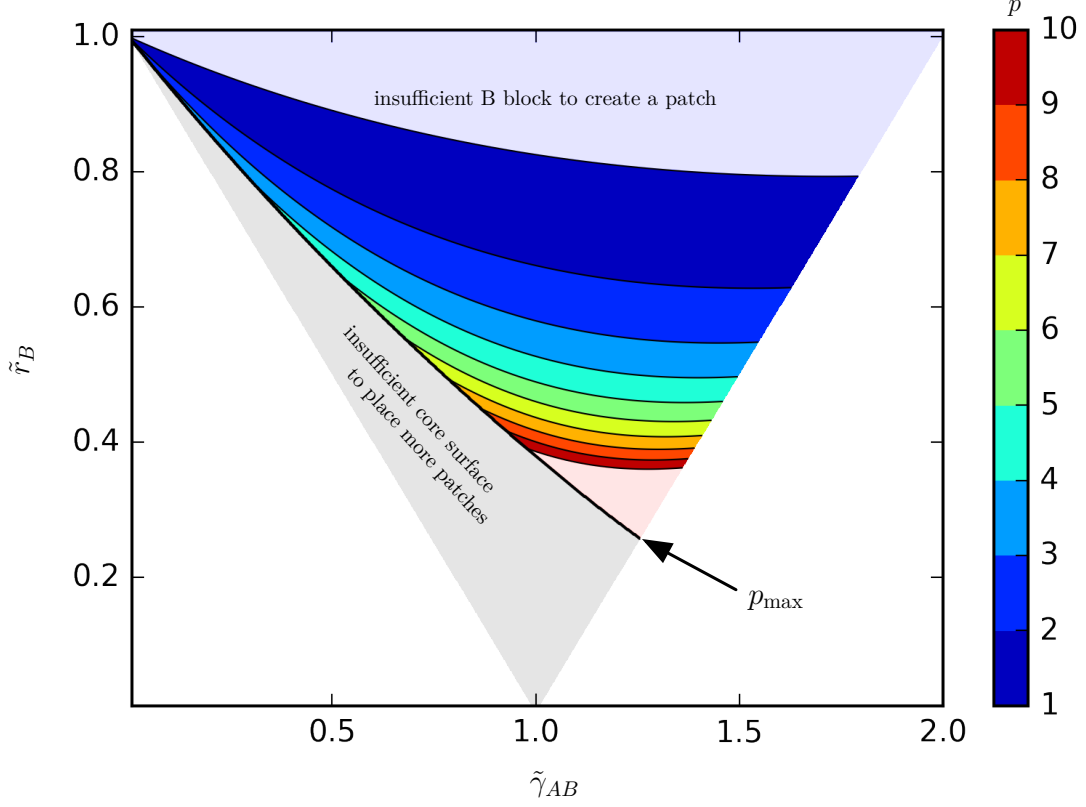


Figure 2: Number of patches p as a function of the dimensionless quantities \tilde{r}_B and $\tilde{\gamma}_{AB}$, at a volume ratio between blocks $V_B/V_A = 0.5$. Critical conditions for the existence of patches that satisfy both force and geometrical conditions are indicated in blue and gray. The upper blue region indicates the insufficient amount of B block to create patches and the gray region corresponds to the condition where all the core surface area is occupied by patches, thus no more patches can be formed. The white regions in the diagram correspond to the condition where the force balance is not satisfied, thus not stable three phases contact line is expected.

where all the surface of the core is occupied by patches, the maximum number of patches p_{\max} can be estimated using (6)

$$p_{\max} = 2(1 + \cos \tilde{\theta}_A)^{-1}. \quad (22)$$

In Figure 2 we present the variation on the number of patches as a function of the dimensionless quantities $\tilde{\gamma}_{AB}$ and \tilde{r}_B for a volume ratio $V_B/V_A = 0.4$. In Figure 2 we depict the limit condition p_{\max} where the surface area of the core is insufficient to allocate more patches. Similarly, we indicate the space parameter region where the amount of the B block is insufficient to satisfy both force and geometrical constrains, thus the formation the patches does not occur.

Since in the main document we proposed an expression that describe the variation on the number of patches as a power law of the parameters $\tilde{\gamma}_{AB}$ and \tilde{r}_B , we evaluate now this approximation using (20) leading to the results presented in Figure 3. In Figure 3 we also present the corresponding predictions for the number of patches given by the scaling proposed in the main document.

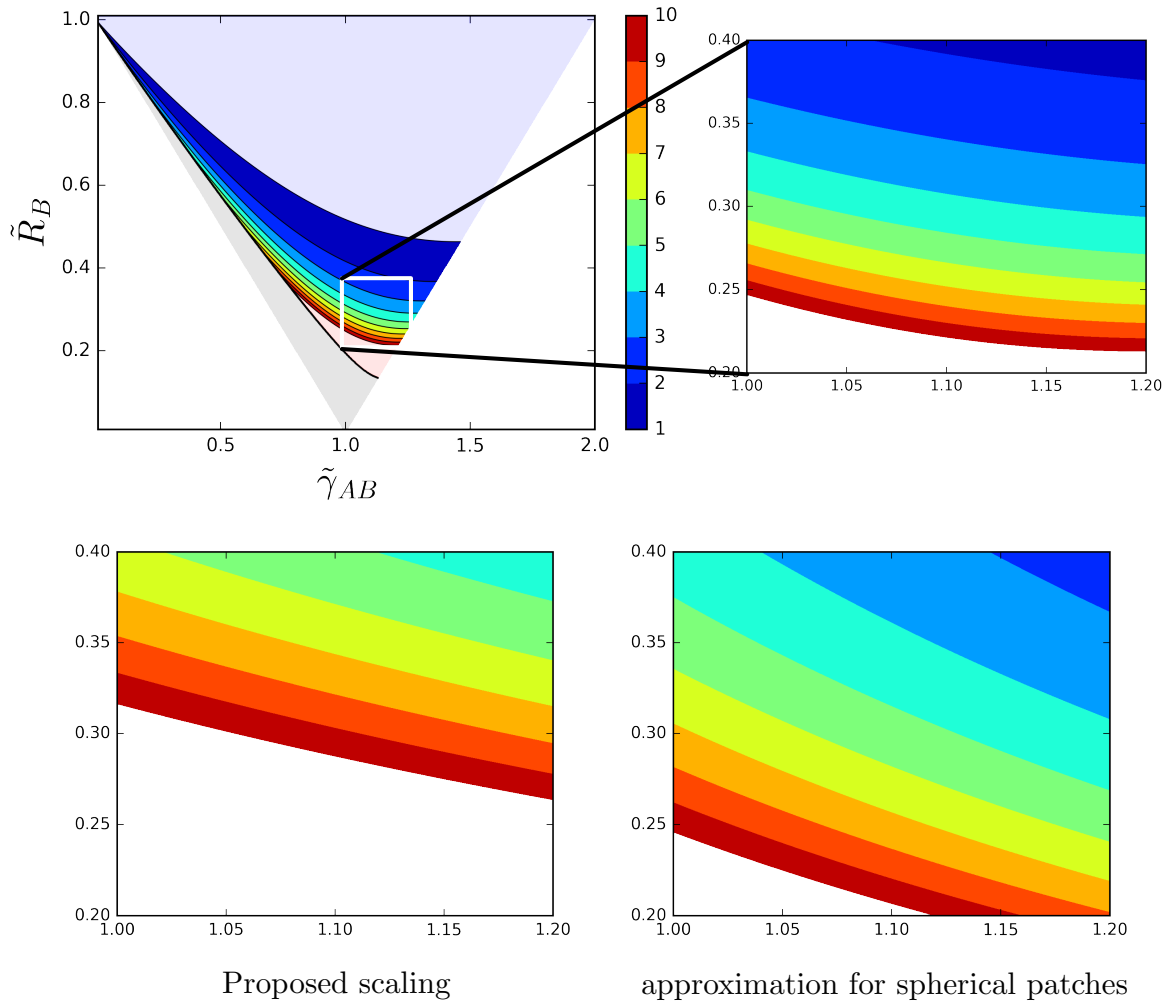


Figure 3: Upper row: number of patches computed from (20) for a volume fraction $V_B/V_A = 0.1$. Lower row: Approximations to the number of patches using the proposed scaling based on simulation results, and the approximation of (20) to similar scaling of the form $\tilde{r}_B^a \tilde{\gamma}_{AB}^b$ in terms of \tilde{r}_B and $\tilde{\gamma}_{AB}$.

Compilation of experimental data

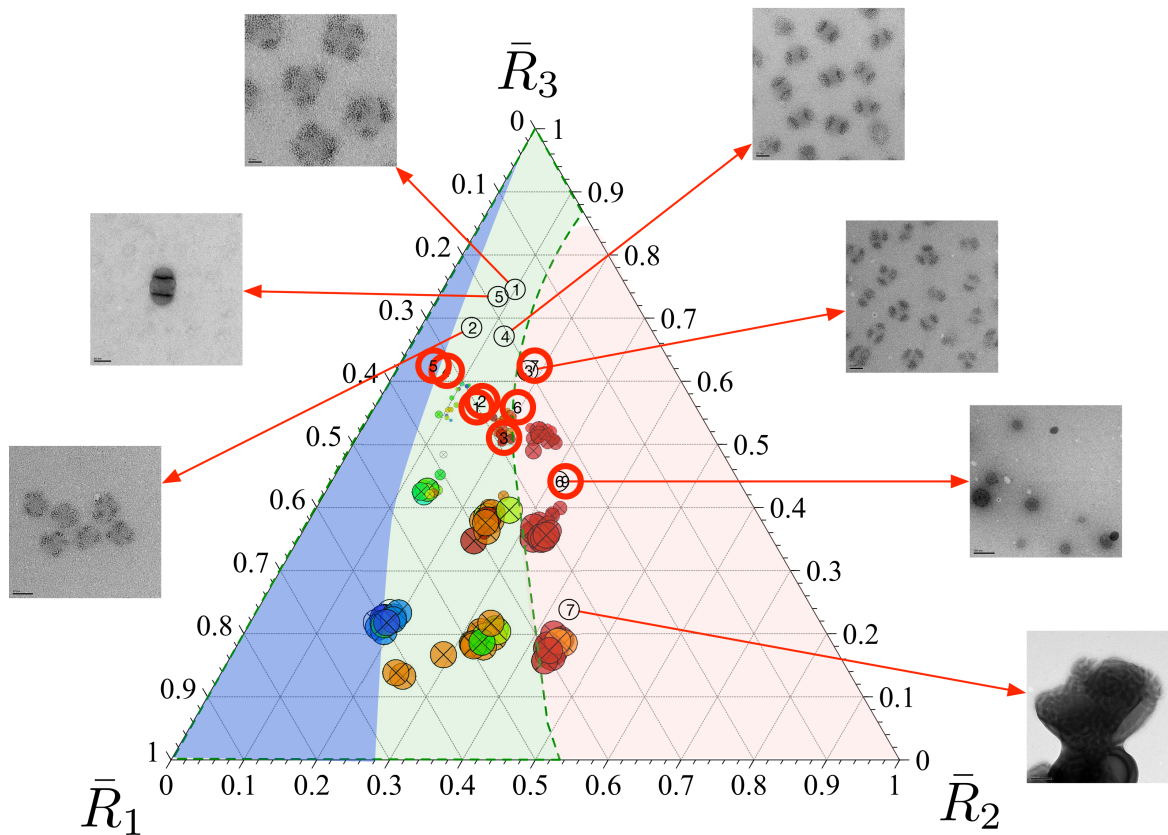


Figure 4: Phase diagram for experimentally reported patchy nanoparticles. Samples identifier with red labels correspond to data reported by [3] and introduced in Table 1. Black identifiers correspond to the experimental conditions used.

PS₂₈₃ - *b* - PIP₃₅₆ - *b* - P2VP₃₅₀

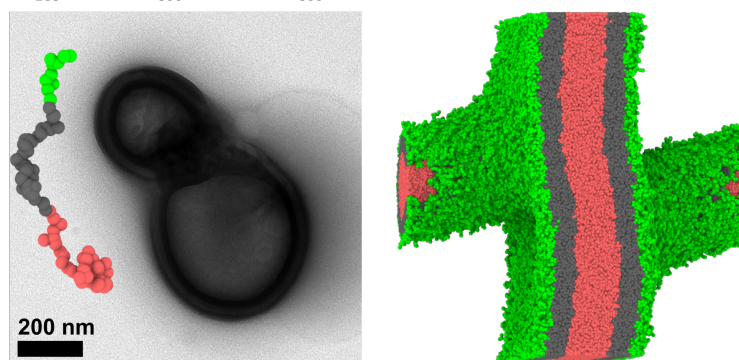


Figure 5: Transmission electron microscopy image for sample SIV2 showing large aggregate with shell forming a continuous phase. We include the results of a simulation where equivalent block copolymer composition leads to continuous phase formation of the middle block

Dissipative particle dynamics

This particle-based method has been applied widely to model block copolymers and colloidal systems [4–6]. A distinguishing feature of the method is that interactions between different constituents are modeled using soft-core potentials, allowing for the modeling of significantly longer time scales relative to atomistic simulations that typically rely on hard-core potentials [7].

In DPD, we describe the system as a set of interacting beads with mass m_i , position \mathbf{r}_i , and velocity \mathbf{v}_i . If \mathbf{f}_i is net force acting on each bead, the kinematic evolution reads $d\mathbf{r}_i/dt = \mathbf{v}_i$, whereas the balance of linear momentum is $m_i d\mathbf{v}_i/dt = \mathbf{f}_i$. In DPD, \mathbf{f}_i has three different contributions and is given by

$$\mathbf{f}_i = \sum_{j \neq i} (\mathbf{F}_{ij}^c + \mathbf{F}_{ij}^d + \mathbf{F}_{ij}^r), \quad (23)$$

where \mathbf{F}_{ij}^c is a conservative force that models pressure effects between particles and spring interactions in chain models, \mathbf{F}_{ij}^d , models dissipative interactions in a fluid, and \mathbf{F}_{ij}^r is a stochastic force accounting for the Brownian motion of polymers and colloids. The dissipative and stochastic forces are given by

$$\mathbf{F}_{ij}^d = -\gamma \omega^d(r_{ij}) \left(\frac{\mathbf{r}_{ij}}{|\mathbf{r}_{ij}|} \cdot \mathbf{v}_{ij} \right) \frac{\mathbf{r}_{ij}}{|\mathbf{r}_{ij}|}, \quad (24)$$

$$\mathbf{F}_{ij}^r = \sigma \omega^r(r_{ij}) \zeta \Delta t^{-1/2} \frac{\mathbf{r}_{ij}}{|\mathbf{r}_{ij}|}, \quad (25)$$

where γ is a friction coefficient, σ is the noise amplitude, ω^d and ω^r are weighting functions, ζ is a random number with zero mean and unit variance. \mathbf{F}_{ij}^d and \mathbf{F}_{ij}^r satisfy the fluctuation-dissipation theorem, which takes the form of the Fokker-Plank equation [8], such that $\omega^d(r_{ij}) = [\omega^r(r_{ij})]^2$, and $\sigma^2 = 2\gamma kT$. k is the Boltzmann constant and T is the equilibrium temperature. The weighting function $\omega^r(r_{ij})$ is assumed to vary linearly away from the particle such that

$$\omega^d(r_{ij}) = [\omega^r(r_{ij})]^2 = \begin{cases} \left(1 - \frac{r_{ij}}{r_c}\right)^2, & r_{ij} < r_c, \\ 0, & r_{ij} \geq r_c. \end{cases} \quad (26)$$

The conservative force accounts for bead-bead \mathbf{F}_{ij}^b , and bead-spring \mathbf{F}_{ij}^s interactions (for connected beads in polymer chains) [9]. We adopt bead-bead and bead-spring contributions of the form

$$\mathbf{F}_{ij}^b = -\frac{du_{ij}^b}{dr_{ij}} \frac{\mathbf{r}_{ij}}{|\mathbf{r}_{ij}|}, \quad (27)$$

$$\mathbf{F}_{ij}^s = -\delta_{ij} \frac{du_{ij}^s}{dr_{ij}} \frac{\mathbf{r}_{ij}}{|\mathbf{r}_{ij}|}, \quad (28)$$

where u_{ij} is a potential energy, $\mathbf{r}_{ij} = \mathbf{r}_i - \mathbf{r}_j$ and $r_{ij} = |\mathbf{r}_{ij}|$. $\delta_{ij} = 1$ if beads i and j are connected, and $\delta_{ij} = 0$ otherwise.

Nanoparticle self-assembly

To construct the library we conduct simulations for different interaction parameters and block compositions N_I/N for $I = A, B$, and C , with N between 25 to 100 beads per chain. We check the nanoparticle morphology at different polymer compositions by changing the total number of chains in the box leading to aggregation numbers z ranging from 100 to 500 chains.

We carry out each simulation in three stages (see Figure 6) in order to reach equilibrated patchy nanoparticles at the given system conditions. This procedure allows us to resemble the experimental methodology proposed by Müller and coworkers [1, 3, 10–12]. This methodology facilitates the prearranging of the polymer segments. On reducing the conformational freedom, the polymer chains can reach equilibrium. In Figure 7 we compare the obtained aggregates using this methodology with respect to a direct mixing of the polymer in the selective solvent.

The chains are initially localized at the center of the box and mixed with a poor solvent for all the blocks. This stage leads to a complete polymer-solvent phase separation. Microphase separation within the polymer phase may occur due to low affinity between blocks. At this point, the morphology of the nanoparticles corresponds to the one obtained for soft confinement in a non-selective wall. The main role of this initial stage is to prescribe a density distribution within the domain, overcoming diffusion of the molecules.

In the second stage we transfer the phase separated blob into a poor solvent for the B block, but selective for the A and C blocks. The swelling of the outer blocks at this stage induces the rearrangement of the domains towards core-corona morphologies or Janus-type nanoparticles for large B . The distributions of the A and C blocks in the corona depend on the relative affinity between blocks ($\chi_{AC}N$).

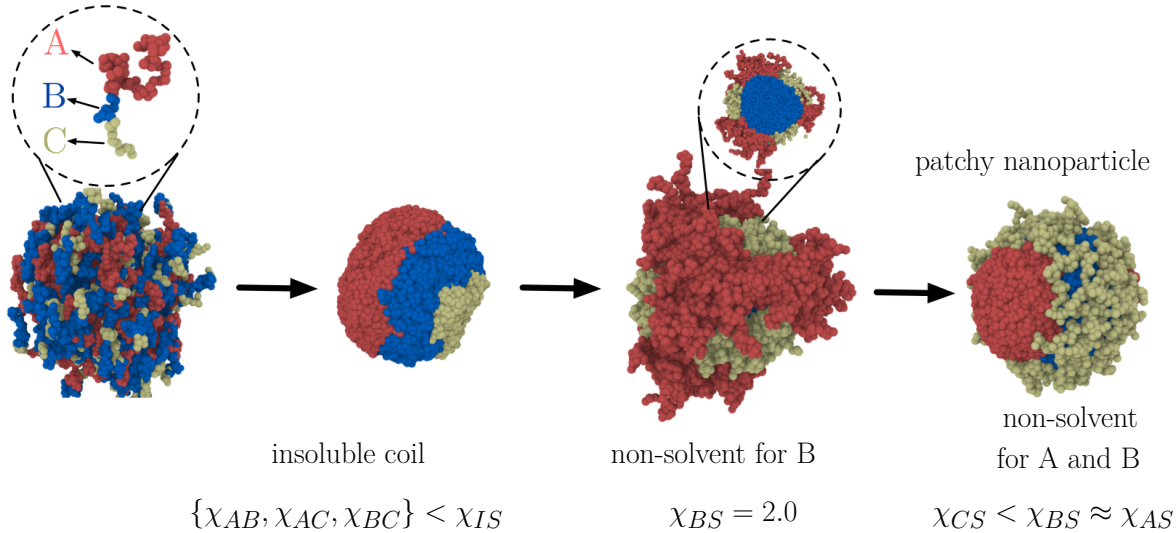


Figure 6: Schematic representation of the triblock terpolymer-solvent mixing stages. Initially, the density distributions in the system are driven by block-block interaction. In the following stages the polymer aggregate is transferred to solvents with different selectivities to induce the formation of core-corona and core-shell-corona, respectively. The solvent selectivities correspond to the ones used experimentally to produce patchy nanoparticles.

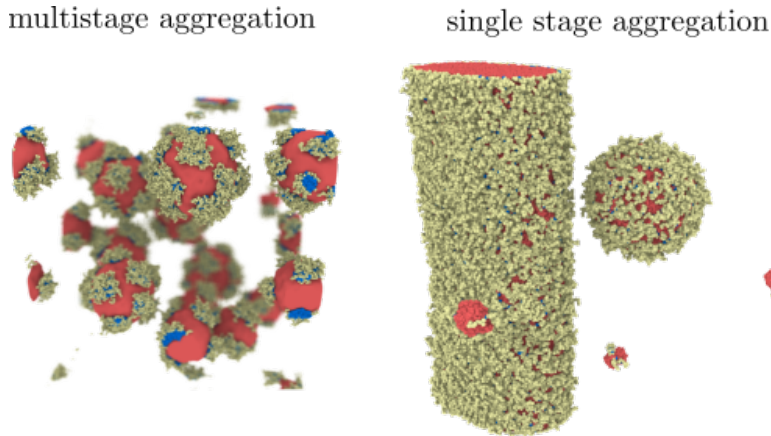


Figure 7: Comparison of the aggregates at equilibrium for multistage and single stage mixing. The multistage procedure allow us to direct the final morphology of the nanoparticle, reducing the conformational degrees of freedom of the polymer coil at each stage.

In the final stage, we place the core-corona nanoparticles in poor solvent condition for the A and B blocks. The blocks now redistribute, forming both A - and B -rich regions, while the soluble block C remains swollen by the solvent. At the end of this stage, the affinity between the species, the size of the blocks, and the topology of the chain, completely dictate the morphology of the nanoparticles. Kinetic effects are implicitly prescribed by the mixing protocol that we use, and account for the path-dependent self-assembly. In our model we neglect entanglement effects and block rearrangement may occur during the simulation time span. This assumption is compatible with the experimental methodology [1, 3, 11], where the structural rearrangements of all the blocks take place due to the low T_g of the middle block and plasticizing effects of the solvent.

Computational characterization of patchy nanoparticles

Radius of gyration

For each block segment we compute the gyration tensor \mathbf{R} to characterize its size. The gyration tensor can be written as

$$\mathbf{R} = \frac{1}{N} \sum_{i=0}^N \mathbf{r}_i \otimes \mathbf{r}_i, \quad (29)$$

where \mathbf{r}_i is the coordinate of the i th bead with respect to the center of mass of the domain, and \otimes denotes the dyadic product. Given the eigenvalues of \mathbf{R} , λ_i with $i = 1, 2, 3$, where $\lambda_1 \geq \lambda_2 \geq \lambda_3$. The radius of gyration of the the segment is given by the ensemble average, $R_g = \langle \lambda_1 + \lambda_2 + \lambda_3 \rangle$.

Interfacial area

To estimate the interfacial area between the different blocks, we use the clustering and surface reconstruction algorithms of the software OVITO [13]. We initially find the clusters of beads formed by A , B , and $A+B$ segments such that beads separated by a distance $r_{\text{clustering}} \leq 1.2r_c$ belong to the same cluster. Next, we identify the associated surface of these regions, Ω_1 , Ω_2 , and Ω_{1+2} . The interfacial area between pair regions are finally computed through $\Omega_{12} = (\Omega_1 + \Omega_2 - \Omega_{1+2})/2$, $\Omega_{23} = \Omega_2 - \Omega_{12}$, $\Omega_{13} = \Omega_1 - \Omega_{12}$. Since the C block is swollen by the solvent, the areas Ω_{I3} correspond to an effective interface formed between the I th block and a mixture of the C block with the solvent.

Experimental characterization of patchy nanoparticles

Transmission electron microscopy

Transmission electron microscopy (TEM) was performed on a JEOL JEM-1230R at an operating voltage of 100 kV. A drop of terpolymer patchy particles dispersion in acetone/isopropanol (5 μ l) was placed on a carbon-coated copper grid. The solvent was immediately blotted by a filter paper underlying the grid. The sample was stained using OsO_4 vapor for 3-4 hours before imaging to selectively stain the butadiene or isoprene block.

Dynamic light scattering

The apparent hydrodynamic radii (R_h) of the patchy nanoparticles in acetone/isopropanol mixtures were measured using a light scattering spectrometer (3D LS spectrometer, LS Instruments) with a He-Ne laser operating at a wavelength of 632.8 nm. The samples were first allowed to pass through a PTFE syringe filter with a pore size of 0.45 μ m before the measurements. The dynamic light scattering (DLS) was probed at 25°C using a scattering angle of 90° and an averaging time of 300 s. Measurements at varying angles were also performed from 30° to 130° in 10° steps with an averaging time of 60 s for each measurement. The obtained autocorrelation functions were analyzed using the cumulant analysis and the CONTIN algorithm to obtain the average hydrodynamic radii ($R_{h,\text{avg}}$) and intensity-weighted distribution of R_h , respectively, via the Stokes-Einstein equation. Viscosities of acetone/isopropanol mixtures at 25°C were obtained on a TVE-25 viscometer (TOKI SANGYO, Japan) using a 0.8° x R24 cone rotor at a rotating speed of 100 rpm.

Table 4: Size [nm] of the core R_1 , shell R_2 , and corona R_3 domains approximated from TEM and DLS measurements. R_1 and R_2 are approximated from the TEM image processing, whereas $R_3 = R_h - (R_1 + 2R_2)$

Code	Name	$2R_1$	$2R_2$	R_3
1	SBM1	24	10	25
2	SBM2	26	6	14
3	SBM3	20	12	6
4	SIM1	22	16	35
5	SIM2	54	11	178
1-1	SBM1	25	9	-
1-2	SBM1	27	10	-

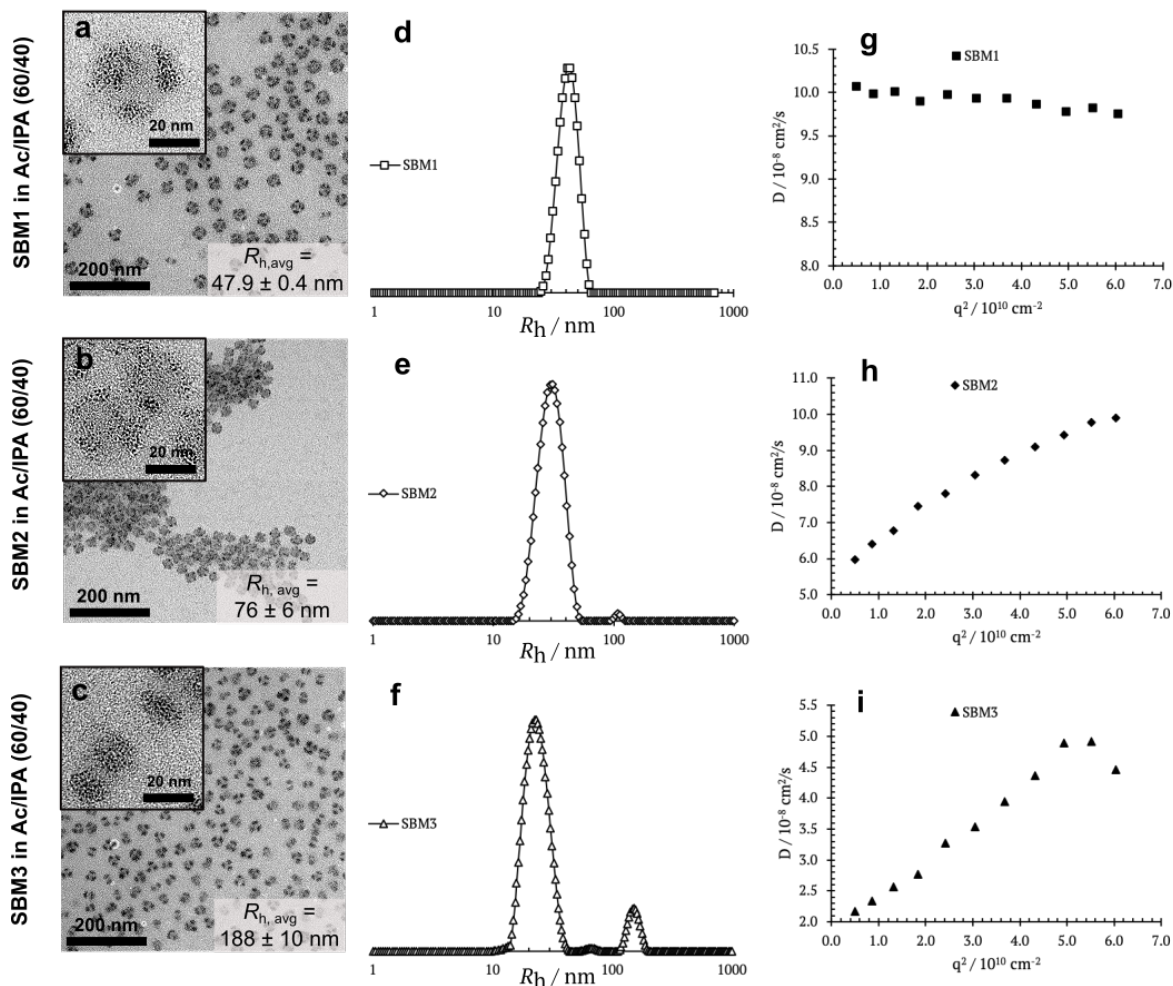


Figure 8: TEM images (a, b, c), intensity-weighted R_h distribution (d, e, f), and the diffusion coefficient, D , versus squared scattering vector, q^2 , (g, h, i) of PS-*b*-PBd-*b*-PMMA (SBM) terpolymers in acetone/isopropanol (Ac/IPA, 60/40). DLS CONTIN plots of SBM1 confirm the formation of multicompartiment micelles (MCMs) with a sharp R_h distribution and $R_{h,avg}$ of around 48 nm. The observed SBM1 R_h is larger than that of SBM2 and SBM3 due to its larger corona size. The SBM1 independency on the scattering angles (D versus q^2) suggests a spherical morphology of the MCMs. On the other hand, both the cumulant analysis $R_{h,avg}$ and the CONTIN plots of SBM2 and SBM3 indicate the formation of larger aggregates of the MCMs in solution due to their shorter corona sizes compared to that of SBM1. The sizes of the individual SBM2 and SBM3 MCMs are around 20 - 30 nm as confirmed by the TEM images and the first-peak observation of the CONTIN plots. However, the calculated $R_{h,avg}$ from the cumulant analysis showed a larger value due to the tendency of the SBM2 and SBM3 MCMs in forming bigger clusters, which are non-spherical as indicated by the high dependency of D on q^2 .

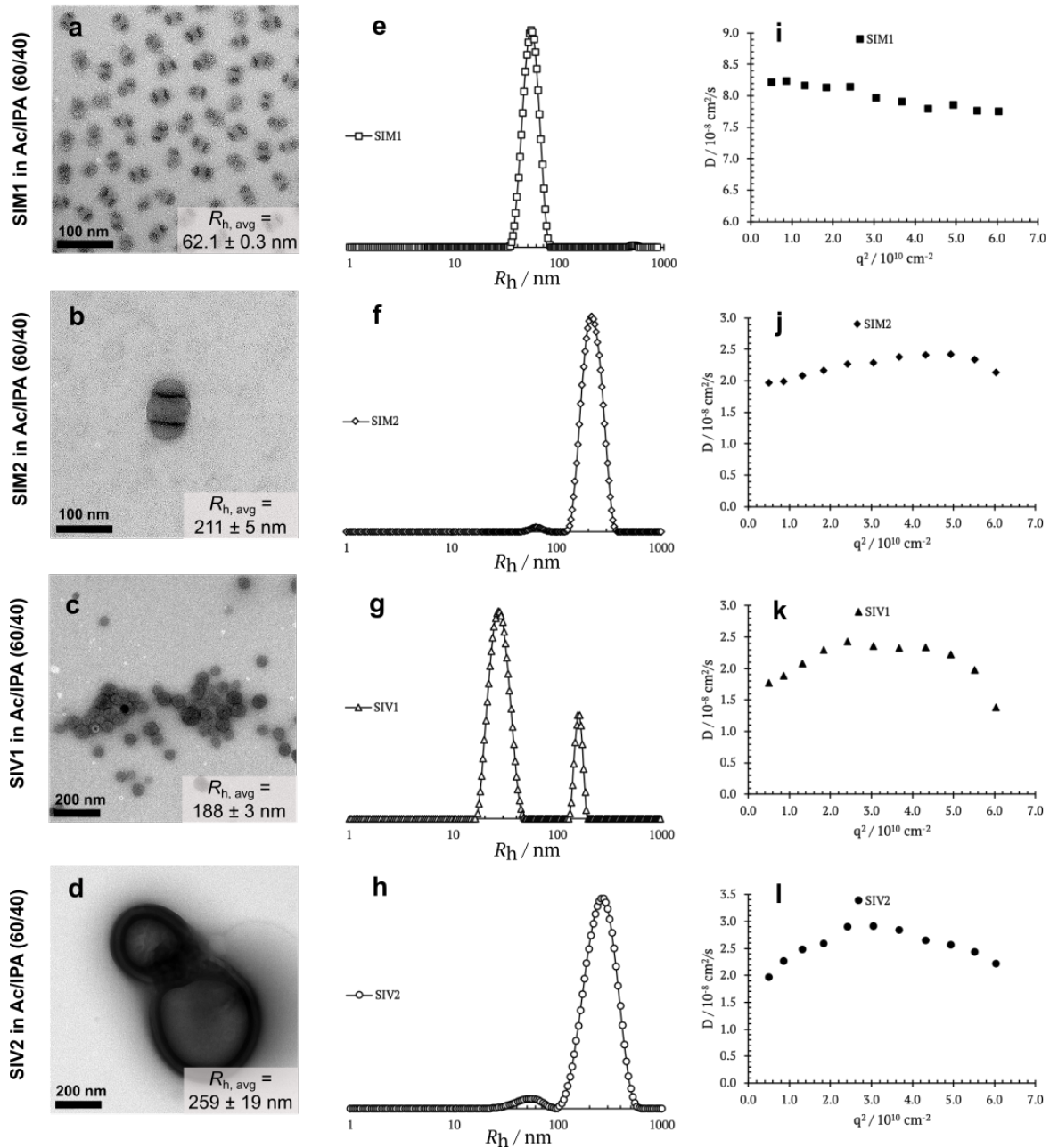


Figure 9: TEM images (a, b, c), intensity-weighted R_h distribution (d, e, f), and the diffusion coefficient, D , versus squared scattering vector, q^2 , (g, h, i) of PS-*b*-PIP-*b*-PMMA (SIM) and PS-*b*-PIP-*b*-P2VP (SIV) terpolymers in acetone/isopropanol (Ac/IPA, 60/40). SIM1 formed stable monodispersed MCMs with $R_{h,avg}$ of around 62 nm as confirmed by the TEM image and the narrow R_h distribution, while SIM2 formed MCMs with a larger size due to its higher molecular weight. The D versus q^2 plots of SIM1 and SIM2 confirm the formation of nearly spherical MCMs indicated by the weak dependency of the scattering data on the scattering angles. More polydisperse MCMs were observed from SIV1 as indicated by the presence of two peaks on the CONTIN plots with $R_{h,avg}$ of around 188 nm, while larger aggregates were observed from SIV2 TEM images and DLS results. A more curved D versus q^2 plot was observed from both SIV1 and SIV2 while having a moderately weak dependency on the scattering angles, indicating nearly-spherical aggregates with some polydispersity and anisotropy.

References

- [1] Tina I. Löbbling, Oleg Borisov, Johannes S. Haataja, Olli Ikkala, André H. Gröschel, and Axel H. E. Müller. Rational design of ABC triblock terpolymer solution nanostructures with controlled patch morphology. *Nature Communications*, 7:12097, jun 2016.
- [2] Charles M Hansen. *Hansen Solubility Parameters: A User's Handbook*. CRC Press, 2nd edition, 2007.
- [3] André H Gröschel, Felix H Schacher, Holger Schmalz, Oleg V Borisov, Ekaterina B Zhulina, Andreas Walther, and Axel H E Müller. Precise hierarchical self-assembly of multicompartment micelles. *Nature communications*, 3:710, jan 2012.
- [4] Haizhou Yu, Xiaoyan Qiu, Nicolas Moreno, Zengwei Ma, Victor M. Calo, Suzana P. Nunes, and Klaus-viktor Peinemann. Self-Assembled Asymmetric Block Copolymer Membranes: Bridging the Gap from Ultra- to Nanofiltration. *Angewandte Chemie*, 2015.
- [5] Robert D. Groot, Timothy J. Madden, and Dominic J. Tildesley. On the role of hydrodynamic interactions in block copolymer microphase separation. *The Journal of Chemical Physics*, 110(19):9739, 1999.
- [6] Effect of affinity on the structure formation in highly size asymmetric bimodal suspensions. *Colloids and Surfaces A: Physicochemical and Engineering Aspects*, 538:481–487, feb 2018.
- [7] Robert D Groot and Patrick B Warren. Dissipative particle dynamics: Bridging the gap between atomistic and mesoscopic simulation. *Journal Chem. Phys.*, 107(11):4423–4435, 1997.
- [8] Pep Español and Patrick B Warren. Statistical Mechanics of Dissipative Particle Dynamics . *Europhysics Letters (EPL)*, 30(4):191–196, 1995.
- [9] N. Moreno, S.P. Nunes, K.-V. Peinemann, and V.M. Calo. Topology and shape control for assemblies of block copolymer blends in solution. *Macromolecules*, 48(21), 2015.
- [10] André H. Gröschel, Andreas Walther, Tina I. Löbbling, Joachim Schmelz, Andreas Hanisch, Holger Schmalz, and Axel H. E. Müller. Facile, Solution-Based Synthesis of Soft, Nanoscale Janus Particles with Tunable Janus Balance. *Journal of the American Chemical Society*, 134(33):13850–13860, aug 2012.
- [11] André H Gröschel, Andreas Walther, Tina I Löbbling, Felix H Schacher, Holger Schmalz, and Axel H E Müller. Guided hierarchical co-assembly of soft patchy nanoparticles. *Nature*, 503(7475):247–51, nov 2013.
- [12] Andreas Walther and Axel H. E. Müller. Janus Particles: Synthesis, Self-Assembly, Physical Properties, and Applications. *Chemical Reviews*, 113(7):5194–5261, jul 2013.
- [13] Alexander Stukowski. Visualization and analysis of atomistic simulation data with OVITO—the Open Visualization Tool. *Modelling and Simulation in Materials Science and Engineering*, 18(1):015012, jan 2010.